# Carbon Nitride Photocatalysts for Water Splitting: A Computational Perspective

Cristina Butchosa, Pierre Guiglion, and Martijn A. Zwijnenburg*

Department of Chemistry, University College London, 20 Gordon Street, London WC1H 0AJ, U.K.

Ⓢ *Supporting Information*

ABSTRACT: We study the thermodynamic ability of carbon nitride materials to act as water splitting photocatalysts using a computational approach that involves a combination of density functional theory (DFT) and time-dependent DFT (TD-DFT) calculations on cluster models of both triazine- and heptazine-based structures. We first use TD-DFT to calculate the absorption spectra of the different cluster models and compare these spectra to those measured experimentally and then calculate using DFT and TD-DFT the reduction potentials of the free electron, free hole, and exciton in these models. We predict that all classes of carbon nitride structures considered should thermodynamically be able to reduce protons and oxidize water. We further provide evidence for the hypothesis that the experimental lack of overall water splitting activity for pure carbon nitride arises from the fact that water oxidation is a four-hole reaction and hence very susceptible to competition with electron−hole recombination. Finally, we propose that the recently reported overall water splitting activity of carbon nitride loaded with polypyrrole nanoparticles arises from a junction formed at the interface of both materials, which assists in keeping electrons and holes apart.
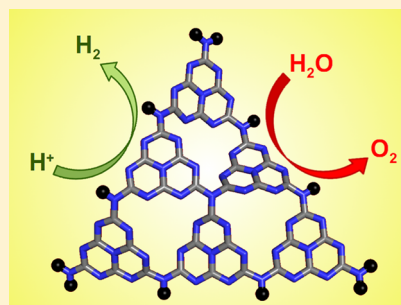
INTRODUCTION

Carbon nitride oligomers and polymers have a fascinating history. A first example of this class of materials with the general formula $(C_3N_3H)_n$ was reported by Berzelius in 1830 and named *melon* by von Liebig not much later in 1834.[1] In the 180 years since, many other related materials with the composition $C_xN_yH_z$ have been prepared, including low-molecular-weight molecules, e.g., *melem* $(C_6N_7(NH_2)_3)$, and high-molecular-weight polymers. In recent years, a large amount of this work has been inspired by the theoretical prediction by Cohen and Liu in 1989[2] that the β-polymorph of hydrogen-free C_3N_4 would be a superhard material and the experimental report of photocatalytic activity of carbon nitrides for water splitting by Antonietti and co-workers in 2009.[3]

Structurally, carbon nitrides are rather complex. While the structures of low-molecular-weight carbon nitride molecules are well-understood (even if only relatively recently[4]), the same does not hold for their polymeric counterparts. Such materials could be based on heptazine (C_6N_7) or triazine (C_3N_3) cores linked together by −NH− bridges to form linear polymer chains (i.e., *melon* in the case of heptazine cores) or by 3-coordinated nitrogen atoms in (partly) polymerized graphitic-like layered structures. While relatively well-characterized samples of *melon*[5] and graphitic-like materials based on heptazine[6,7] and triazine[8] have been reported in the literature, the structure of many materials relevant to applications discussed above is only poorly understood. Samples are often poorly crystallized or amorphous, meaning that only limited information can be extracted through X-ray diffraction and/or NMR. Equally, measurement of the mass percentage of hydrogen is often difficult due to adsorbed water. As a result,

analysis of the H/C ratio to distinguish, for example, between linear polymers and graphitic-like structures, is difficult. Finally, shifts in the UV−vis spectra with synthesis temperature[3] suggest that the optical properties, key to important applications of carbon nitrides, might also help with understanding their structure.

As alluded to above, carbon nitride can act as a photocatalyst for the splitting of water into molecular hydrogen and oxygen by facilitating the reduction of protons to hydrogen gas. After the work of Antonietti and co-workers,[3,9] itself partly inspired by earlier work on the photocatalytic activity of poly(p-phenylene),[10−12] there was a flurry of work on (doped) carbon nitride materials as photocatalysts.[13−22] A large number of these materials only act as photocatalysts for the proton reduction half-reaction (A) and currently do not perform the four-electron water oxidation half-reaction (B):

$$2H^+ + 2e^- \rightarrow H_2 \qquad \text{(A)}$$

$$O_2 + 4H^+ + 4e^- \rightarrow 2H_2O \qquad \text{(B)}$$
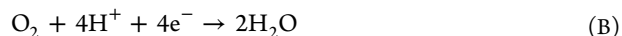
Some other carbon nitride materials can catalyze both half-reactions but not simultaneously in the same experiment. Above, in line with convention, both half-reactions are written as reductions. However, in the case of water splitting, half-reaction B will run in the opposite direction.

Because of their apparent inability to drive reactions A and B simultaneously, carbon nitride materials in general cannot split

pure water and their activity for proton reduction is typically measured in the presence of a sacrificial electron donor, for example methanol, which is oxidized instead of water in a two-electron oxidation to formaldehyde (C):

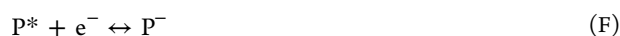$$CH_2O + 2H^+ + 2e^- \rightarrow CH_3OH \qquad (C)$$
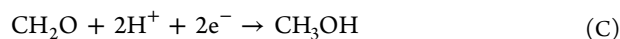
Similarly, water oxidation activity, when studied, is normally measured in the presence of a sacrificial electron acceptor, for example, the silver cations of a silver nitrate solution, which, in that case, are reduced to metallic silver.

Recently, however, a carbon nitride material loaded with polypyrrole nanoparticles on its surface was reported to split pure water into hydrogen and hydrogen peroxide.[18] Here, water appears to be oxidized in a two-electron reaction to hydrogen peroxide (D), something that is reported not to happen in the absence of the polypyrrole nanoparticles or by the polypyrrole nanoparticles on their own:

$$H_2O_2 + 2H^+ + 2e^- \rightarrow 2H_2O \qquad (D)$$
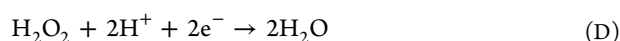
After the absorption of light by the carbon nitride material, electrons are excited from the top of the valence band to the bottom of the conduction band and excitons, bound electron–hole pairs, are formed. These excitons can subsequently be split into free holes in the valence band and free electrons in the conduction band, where free signifies that they are not bound in a neutral exciton. The free electrons can drive the reduction of protons (reaction A), the free holes, the oxidation reactions (reactions B–D), while the exciton can act as both reductant and oxidant. Following our previous work,[23] the relevant half-reactions, again written in line with convention as reductions, are

$$P^+ + e^- \leftrightarrow P^* \qquad (E)$$

$$P^* + e^- \leftrightarrow P^- \qquad (F)$$

$$P + e^- \leftrightarrow P^- \qquad (G)$$

$$P^+ + e^- \leftrightarrow P \qquad (H)$$

Here, P stands for the neutral carbon nitride photocatalyst, P* for the excited photocatalyst (i.e., the exciton), and P⁻/P⁺ for the photocatalyst with a free electron or free hole. In the remainder of the paper, we will refer to the latter three simply as exciton, free electron, and free hole. In half-reactions E and G, the exciton and free electron act as reductants; the carbon nitride photocatalyst donates electrons and the half-reaction will run in the opposite direction to that written above. In the other two half-reactions, the exciton and free hole act as oxidants, with the carbon nitride accepting electrons. The free energy change of reactions E–H (and also A–D) can be expressed in terms of the associated reduction potential, the potential difference relative to a standard electrode, typically the standard hydrogen electrode (SHE), thermodynamically required to run the half-reaction as a reduction.

The reduction potential of half-reaction H can be referred to as the ionization potential (IP), as it equals the energetic cost of extracting an electron from the top of the carbon nitride valence band. Equally, the reduction potential of half-reaction G can be thought of as the materials' electron affinity (EA), the energy released upon adding an electron to the bottom of the conduction band of carbon nitride. The reduction potentials of half-reactions E an F, finally, are, respectively, the excited state ionization potential and electron affinity (IP* and EA*).[23]

Having defined the reduction potentials of the water splitting reactions (A–B, D), the sacrificial electron donors (C) and the carbon nitride in its different states (E–H), one can then analyze the thermodynamic ability of the carbon nitride to drive the water splitting reactions when illuminated.[23] For proton reduction to be feasible in the presence of the carbon nitride, the reduction potential of the free electron (EA) and/or exciton (reaction IP*) in carbon nitride should be more negative than the reduction potential of reaction A. Equally, for any of the oxidation reactions to be thermodynamically feasible, the reduction potential of the carbon nitride free hole (IP) and/or exciton (reaction EA*) should be more positive than the reduction potential of reactions B, C, and/or D. Graphically, this means that EA/ IP* and IP/EA* potentials should straddle the reduction potentials of reactions A–D, as illustrated in Figure 1.
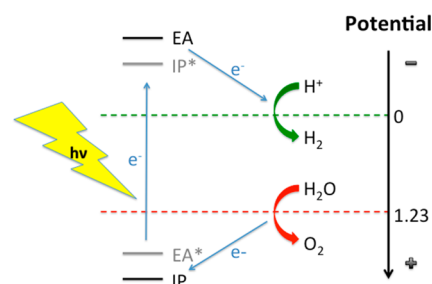
Figure 1. Scheme showing how the (standard) reduction potentials of the ideal photocatalyst straddle the proton reduction and water oxidation potentials.

In our previous work on poly(p-phenylene)[23] (PPP) polymer chains, a material known to only catalyze the reduction of protons and not the oxidation of water, we showed that PPP is thermodynamically unable to oxidize water. The IP and EA* of PPP were predicted to be more negative than the potential of the water oxidation reaction at pH 0 and only marginally more positive at higher pH values. Moreover, we demonstrated that the IP and EA* of PPP are predicted to be considerably more positive than the reduction potential of triethylamine oxidation, the sacrificial electron donor used experimentally. While this explains the lack of water oxidation activity for PPP, preliminary calculations on very simple heptazine-based cluster models of carbon nitride in the same work predict that IP and EA* of carbon nitride might be considerably more positive than the standard reduction potential of the water oxidation reaction. Oxidation of water thus appears to be strongly exothermic in the case of carbon nitride, as is the reduction of protons, suggesting that the inability to split pure water in this case is kinetic rather than thermodynamic in origin.

In this paper, we revisit the standard reduction potential of the charge carriers and excitons in carbon nitride and their ability to reduce protons and oxidize water. We perform calculations on a range of carbon nitride cluster models (see Figure 2), including both linear and graphitic structures, based on both heptazine and triazine cores. We also predict the absorption spectra of these carbon nitride models and compare them to experimental data. In all of these calculations, we carefully explore the effect of both the remainder of the material around the cluster model, i.e., stacking effects and noncovalent interactions with the cluster model, and the environment the materials is embedded in, e.g., solvent, on the optical and redox properties. Finally, we discuss a possible physical mechanism
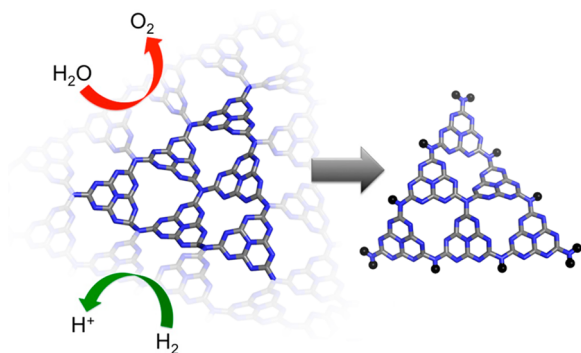
Figure 2. Link between material, left, and cluster model structure, right. Atoms represented as black spheres indicate where the cluster model would connect to the remainder of the material.

explaining why, in the presence of polypyrrole nanoparticles, carbon nitride is able to split pure water.

■ COMPUTATIONAL DETAILS

Ground State Structures. For every cluster model, first an initial conformational search was performed using the OPLS-2005 forcefield[24] and a low-mode sampling algorithm.[25] We typically used a combination of 10 000 search steps and minimum and maximum low-mode move distances of 3 and 20 Å, respectively. All the structures located within an energy window of 200 kJ/mol relative to the lowest energy conformer were saved. The lowest energy conformers of each cluster were subsequently reoptimized using DFT and a combination of the B3LYP[26−29] XC-potential and the DZP[30] basis set.

Optical Spectra. Vertical absorption spectra were calculated for the ground state geometries of the different cluster models using TD-DFT. All calculations used the same XC-potential and basis set as the ground state calculations and furthermore made the Tamm−Dancoff approximation[31] to TD-DFT. For selected systems, we compared the TD-B3LYP results with those obtained using the approximate coupled cluster RI-CC2[32] method. The RI-CC2 calculations employed the def2-SVP[30] basis set and made the frozen core approximation. Finally, we calculated for selected systems also the Λ diagnostic of Peach et al.[33] The Λ diagnostic characterizes for an excitation the overlap between the involved occupied and unoccupied orbitals and is an indicator of potential issues with describing this excitation by TD-DFT due to it having a charge-transfer (CT) nature. The Λ scale ranges from 0 (no overlap, CT excitation) to 1 (full overlap, fully local excitation), and for excitations with $\Lambda > 0.3$, TD-B3LYP has been found to normally not suffer from any CT problems for organic molecules.[33]

Redox Potentials for Carbon Nitride. The IP, EA, IP*, and EA* of the different carbon nitride cluster models were calculated from half-reactions E−H. First, the adiabatic free-energy differences of the reactions were calculated and then, subsequently, the reduction potentials were obtained via

$$E^0(x) = -\frac{\Delta G(x)}{nF} \tag{1}$$

where n is the number of electrons involved in the half-reaction and F the Faraday constant.

The adiabatic free energies of all the relevant species can be considered as a sum of three contributions:

$$G(x) = U(x) + G_{\text{vib}}(x) + G_{\text{sol}}(x) \tag{2}$$

Here, $U(x)$ is the electronic energy of species x, $G_{\text{vib}}(x)$ the contribution of vibration, rotation, and translation to the free energy, and $G_{\text{sol}}(x)$ the free energy contribution due to solvation and the environment in general.

$U(x)$ is obtained from DFT (B3LYP) ground state energy minimization in the case of P, P⁻, and P⁺, and from a TD-DFT (TD-B3LYP) S_1 excited state energy minimization for P*. $G_{\text{vib}}(x)$ can be obtained from frequency calculations on the minima obtained through DFT and TD-DFT. We, however, set $G_{\text{vib}}(x)$ to zero for the carbon nitride structures, as calculating the frequencies can be very costly for the larger systems, especially in the case of P*, and because explicit calculations of $G_{\text{vib}}(x)$ for selected carbon nitride systems (also in our previous work[23]) show that the contribution of this term to the free-energy differences and potentials is normally very small (<0.1 (e)V). $G_{\text{sol}}(x)$, the effect of solvent and the environment in general, is obtained, finally, through the use of the COSMO dielectric continuum solvation model.[34−36]

Within the COSMO model, the properties of the environment are characterized by its relative dielectric permittivity (ε). All calculations, except in few cases where explicitly stated, are performed for the case of $\varepsilon = 80.1$, solvation in water. In reality, the environment of the carbon nitride material will be more complicated than merely water, but we believe that this is a good approximation, also because we know from our previous work[23] that the potentials are relatively insensitive to the precise value of ε used. In the case of P, P⁺, and P⁻, we calculate $G_{\text{sol}}(x)$ for the solvated minimum obtained after a full COSMO geometry optimization. For P*, we instead perform single-point COSMO calculations on the gas phase minimum energy structures, as no COSMO gradients are available in the code we use for TD-DFT.

Finally, in the case of stacked structures, in general, vertical rather than adiabatic potentials were calculated. The geometries of the stacked structures are those of gas phase minimum energy structures of individual clusters stacked by stacking distances taken from experiment.

Redox Potentials for Water and Sacrificial Electron Donors. We include all terms of equation 2 when calculating the potentials for water and the sacrificial electron donors. Because the structures of the product and reactants in half-reactions A−D are generally very different, their vibrational spectra are generally rather different, and as a result, the contribution of $G_{\text{vib}}(x)$ is not negligible for these potentials and explicitly calculated. Solvation is always included with the relative dielectric permittivity of water. The free energy of protons $G(\text{H}^+)$, which enters in all water and sacrificial electron donor potentials, is calculated from the experimental value of the absolute potentials of the standard hydrogen electrode ($E_{\text{abs}}(\text{SHE}) = 4.44$ V,[37,38] $\Delta G(\text{SHE}) = -4.44$ eV) using

$$G(\text{H}^+) = -\Delta G(\text{SHE}) + \frac{1}{2}G(\text{H}_2) \tag{3}$$

where $G(\text{H}_2)$ is the free energy of molecular hydrogen. We choose to base $G(\text{H}^+)$ on experimental information rather than calculating it from first principles, as the latter is complicated and error prone.[39,40] Finally, where available, we take the values of the redox potentials for water and sacrificial electron donors from our previous work.[23]

Codes. All DFT, TD-DFT, and RI-CC2 calculations were performed using Turbomole 6.5,[41−44] except for the calcu-

lations of the Λ values, which were performed using GAMESS-US (version 1, October 2010 R1).[45] Conformer searches were performed in MacroModel 9.9.[46]

■ RESULTS AND DISCUSSION

Spectra of Heptazine-Based Materials. Before discussing the absorption spectra of different heptazine-based materials in detail, we first compare the predictions of TD-B3LYP with those obtained using RI-CC2. Figure 3 shows the
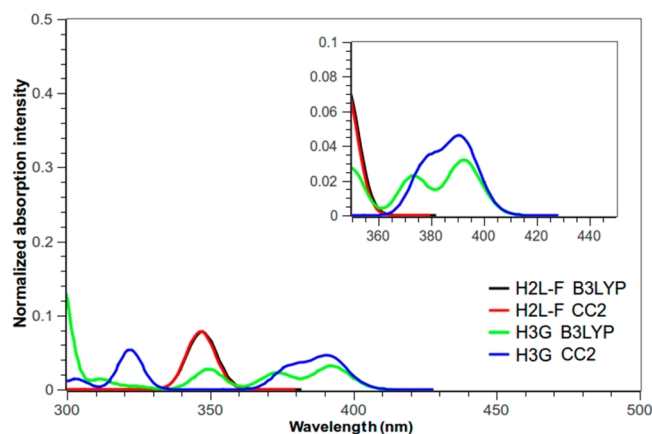

Figure 3. Comparison of the TD-B3LYP and RI-CC2 spectra of the H2L-F linear *melem* dimer and H3G 3-ring graphitic cluster models.

TD-B3LYP and RI-CC2 spectra of the H2L linear *melem* dimer and the H3G 3-ring graphitic structure (see Figures 4 and 5 for
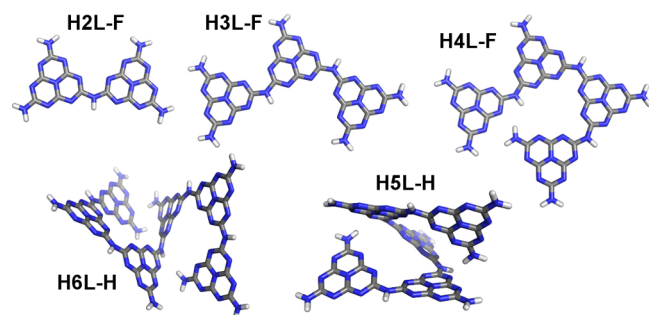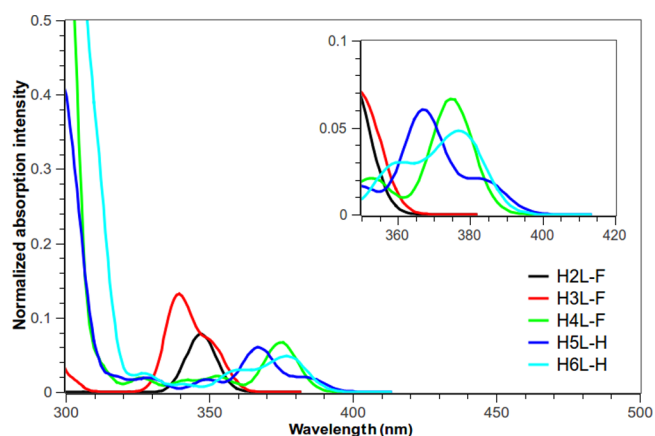

Figure 4. Cluster models of linear heptazine-based structures. The suffix F indicates a flat conformer, while the suffix H is used to label helical conformers.
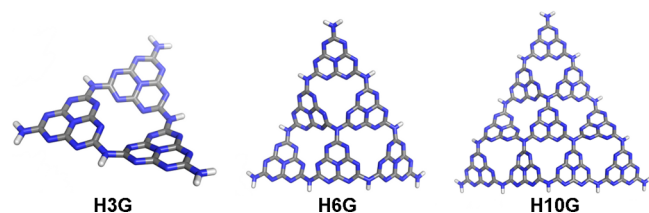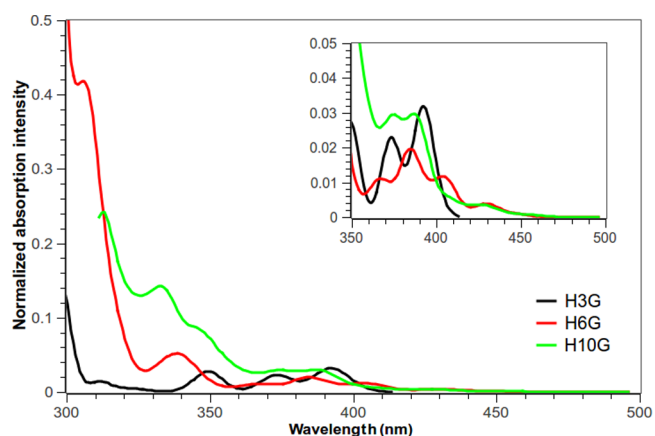

Figure 5. Cluster models of graphitic heptazine-based structures.

an overview of heptazine cluster structures). For both clusters, there is a very good agreement for the first absorption peak. In line with this good agreement between TD-B3LYP and CC2, we also find that the Λ values of the lowest excitations are consistently larger than 0.3 and that, hence, charge-transfer excitations are unlikely to be an issue when describing these systems with TD-B3LYP.

Figures 6 and 7 show the TD-B3LYP spectra of linear and graphitic heptazine-based clusters, respectively. We consider

Figure 6. TD-B3LYP spectra of the lowest energy conformers of cluster models of linear heptazine-based structures.

Figure 7. TD-B3LYP spectra of the lowest energy conformers of the cluster models of graphitic heptazine-based structures.

linear structures of up to 6 heptazine units (H2L-H6L) and triangular cuts of a graphitic structure containing up to 10 heptazine units (H3G, H6G, and H10G). The lowest energy conformers of the longer linear *melem* chains (H5L, H6L) are helical, but flat conformers exist and show very similar spectra, only with increased intensity at long wavelengths (see Figures S1 and S2 in the Supporting Information). Similarly, helical conformers of the shorter H3L and H4L linear *melem* chains have very similar spectra to their respective flat conformers (see Figures S3−S6 in the Supporting Information). The graphitic structures tend to be nonplanar and buckled, similar to what was observed in previous periodic DFT calculations on extended graphitic heptazine-based sheets.[47] For both classes of materials, the overall absorption spectra red shift upon increasing the number of heptazine units. The absorption on-set, the wavelength of the first absorption feature, for the graphitic structures is always more red-shifted than those of the linear structures. For example, the absorption on-set of H6L is 380 nm, whereas that of H6G lies at 450 nm. Stacking of the graphitic structures, finally, is predicted to lead to a minor further red shift (explicitly calculated for AA and AAA stackings of H3G using an interlayer distance of 3.4 nm taken from experiment,[6] yielding a red shift of ∼20 nm; see Figures S7 and S8 in the Supporting Information).

The spectra in Figures 6 and 7 appear to be essentially converged with cluster size and span a similar wavelength range as experimental absorption spectra of carbon nitride materials thought to be based on heptazine cores.[3,15] Slightly depending on the exact preparation conditions, materials synthesized at low temperatures (400−550 °C) have an absorption on-set in between 350 and 400 nm, whereas, in materials prepared at higher temperatures (600−650 °C), this peak red shifts to above 400 nm and a new lower-intensity shoulder appears in the 425−550 nm range. At the same time, the C/N ratio increases and the H/C ratio decreases.[15] A comparison of these experimental observations with our predicted spectra suggests that this change in absorption spectra with synthesis temperature could be explained by a conversion of linear *melem* structures into a graphitic material through further condensation.

Spectra of Triazine-Based Materials. In the case of the triazine-based materials, we focus on graphitic structures (see Figure 8 for an overview of the considered cluster models of the
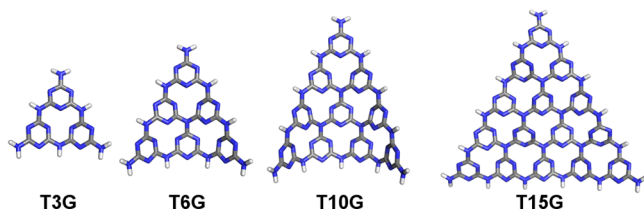

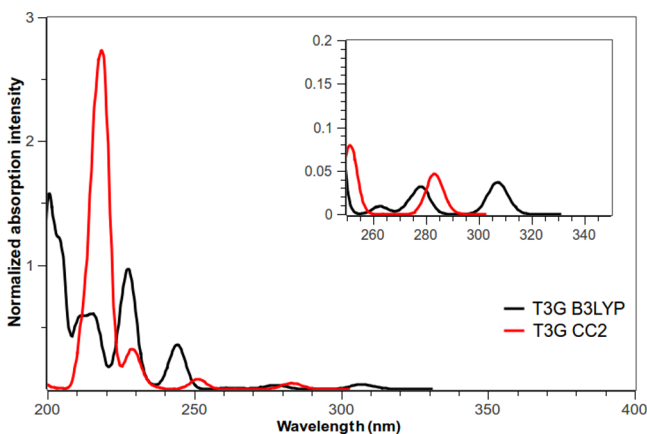**Figure 8.** Cluster models of graphitic triazine-based structures.

Figure 9. Comparison of the TD-B3LYP and RI-CC2 spectra of the T3G 3-ring graphitic cluster model.

triazine-based structures). Figure 9 shows the TD-B3LYP and RI-CC2 spectra of the T3G 3-ring graphitic triazine structure. There is a reasonable agreement between the RI-CC2 and TD-B3LYP, where the latter is consistently red-shifted by approximately 25 nm with respect to the former. The Λ values of the excitations are consistently larger than 0.4, and hence, it is unlikely that the red shift arises from an issue with describing charge-transfer excitations. All the larger cluster models are just like the graphitic heptazine-based cluster models, nonplanar and buckled, again similar to what was observed in previous periodic DFT calculations on extended sheets.[47]

Figure 10 shows the TD-B3LYP spectra of the graphitic triazine-based materials. We consider triangular cuts of a
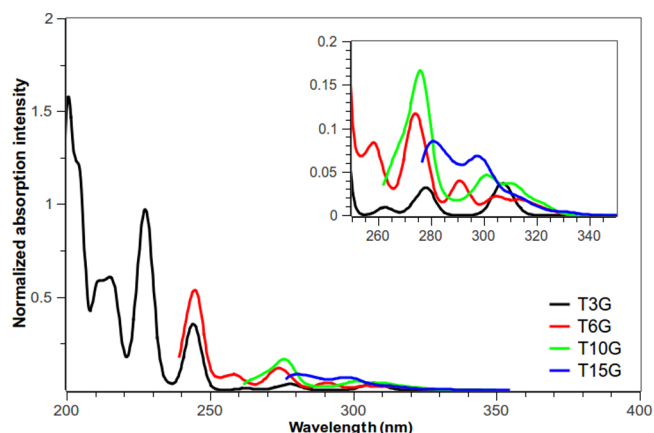

Figure 10. TD-B3LYP spectra of the lowest energy conformers of the cluster models of graphitic triazine-based structures.

graphitic structure containing up to 15 triazine units (T3G, T6G, T10G, and T15G). Just as observed for the heptazine clusters, the absorption on-set red shifts with increasing number of triazine units in the cluster and converges to a value of approximately 330 nm. Based on single layers, our calculations thus predict that triazine-based materials should have a blue-shifted absorption spectrum compared to heptazine-based materials. Stacking of the graphitic structures, again, is predicted to lead to a minor further red shift. Explicit calculations for AA, AAA, and AAAA on-top stackings of T3G and T6G using an interlayer distance of 3.28 nm taken from experiment[8] yield a red shift of ∼20 nm in the spectrum. The lowest excitations of the larger clusters are even further red-shifted, by ∼40 nm, but these excitations have negligible excitation strength (see Figures S9 and S10 in the Supporting Information). The latter might be the result of interactions between monomer excitations with transition dipole moments perpendicular to the stacking direction, similarly as we previously observed for organic triazine-based polymers.[48] Therefore, stacking does not appear to change the prediction that graphitic triazine should have a blue-shifted absorption spectrum compared to heptazine-based materials. This is at odds with the recently reported experimental absorption spectrum of graphitic triazine-based material,[8] which is significantly red-shifted to the experimental heptazine-based material spectra. The origin of this discrepancy is unclear. As discussed above, the match between TD-B3LYP and RI-CC2 is reasonable and, if anything, would suggest that the TD-B3LYP spectra is red-shifted too much, while stacking is predicted to result in a red shift, but not of big enough magnitude to reproduce experiment. One possible explanation is that this might be the result of another stacking scheme beyond simple on-top stacking. There is indeed some experimental evidence for AB or ABC stacking in the experimental samples. An alternative explanation is the presence of nitrogen vacancies in the experimental graphitic triazine samples. Such vacancies have recently been reported to result in the appearance of a new absorption shoulder in the 450−600 nm range.[49]

Carbon Nitride Potentials. Having discussed the carbon nitride spectra, we now focus on the carbon nitride potentials. Figures 11 and 12 show the predicted reduction potentials for free electrons, free holes, and excitons in isolated linear and graphitic heptazine-based carbon nitride structures in water (ε = 80.1) at pH 7 (see Figures S11 and S12 in the Supporting Information for the same potentials at pH 0). For comparison,
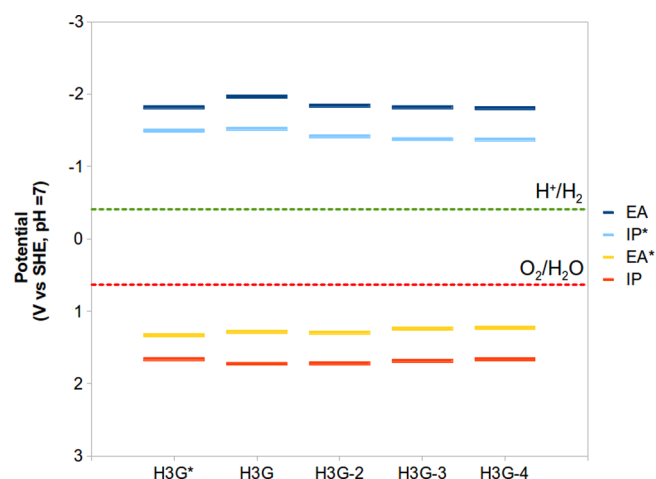
Figure 11. (TD-)B3LYP predicted IP, EA, IP*, and EA* adiabatic potentials of the lowest energy conformers of cluster models of linear heptazine-based structures in water ($\varepsilon = 80.1$) at pH 7 (see Figure S11 in the Supporting Information for the pH 0 equivalent).
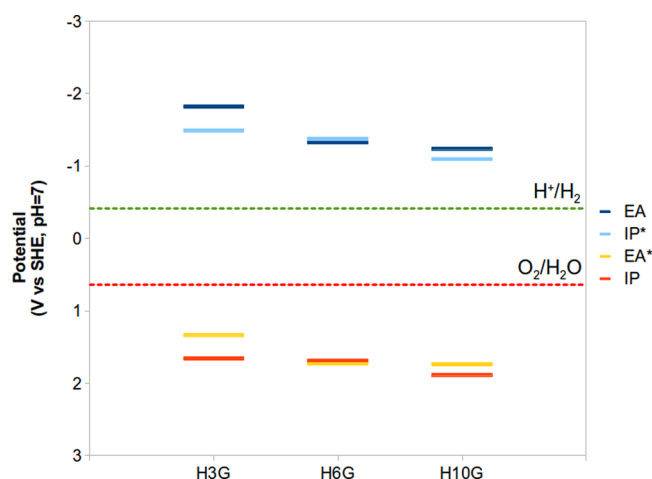
Figure 12. (TD-)B3LYP predicted IP, EA, IP*, and EA* adiabatic potentials of the cluster models of graphitic heptazine-based structures in water ($\varepsilon = 80.1$) at pH 7 (see Figure S12 in the Supporting Information for the pH 0 equivalent).

all figures also show the predicted hydrogen reduction and water oxidation potentials. For pH 7, these latter potentials have been shifted using the Nernst equation to reflect the change in pH away from 0. From Figures 11 and 12, it is clear that our calculations predict that, in line with our preliminary work on smaller clusters,[23] the two classes of heptazine-based materials considered have a significant thermodynamic driving force for both proton reduction and water oxidation. Calculations for the graphitic structures that take into account the effect of stacking, using the same H3G stacks as used to probe the effect of stacking on the spectra above, suggest that the further effect of stacking on the graphitic heptazine-based materials is small (see Figure 13). In this case, in order to preserve the experimental stacking distance, the latter potentials are by necessity vertical rather than adiabatic potentials (Figure 13 for comparison also shows the adiabatic potential of the isolated H3G).

In the case of the linear structures, the free electron and hole potentials in Figure 12 are similar to the Kohn−Sham band positions relative to the absolute vacuum level previously

Figure 13. (TD-)B3LYP predicted IP, EA, IP*, and EA* vertical potentials of stacks of H3G ($\varepsilon = 80.1$) at pH 7. Adiabatic potentials of isolated H3G (H3G*) are also shown for comparison.

calculated for infinite linear *melon* chains.[3] The main differences are that our predicted free electron potential is slightly more negative than the bottom of the conduction band of the infinite chain and our predicted free hole potential slightly more positive than the top of the valence band of the infinite chain. The origin for these minor discrepancies probably is a combination of the fact that the top of the valence band and bottom of conduction band are only approximations to the adiabatic free electron and hole potentials and the use of the PBE functional in ref 3, which is known to underestimate energy gaps.

Figure 14 shows the predicted reduction potentials for free electrons, free holes, and excitons in isolated graphitic triazine-
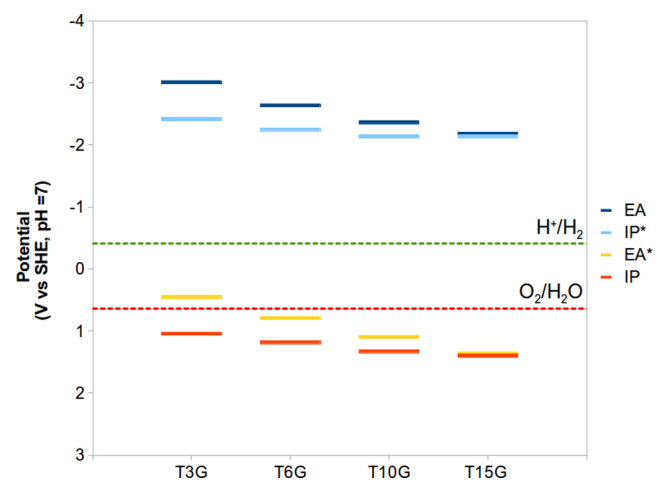
Figure 14. (TD-)B3LYP predicted IP, EA, IP*, and EA* adiabatic potentials of the cluster models of graphitic triazine-based structures in water ($\varepsilon = 80.1$) at pH 7 (see Figure S13 in the Supporting Information for the pH 0 equivalent).

based carbon nitride structures in water ($\varepsilon = 80.1$) at pH 7 (see Figure S13 in the Supporting Information for the same potentials at pH 0). The triazine-based structures have a larger thermodynamic driving force for proton reduction than the heptazine-based structures, but water oxidation is predicted to be less exothermic. The effect of stacking, shown in Figure 15 for T3G, appears larger for triazine-based frameworks.
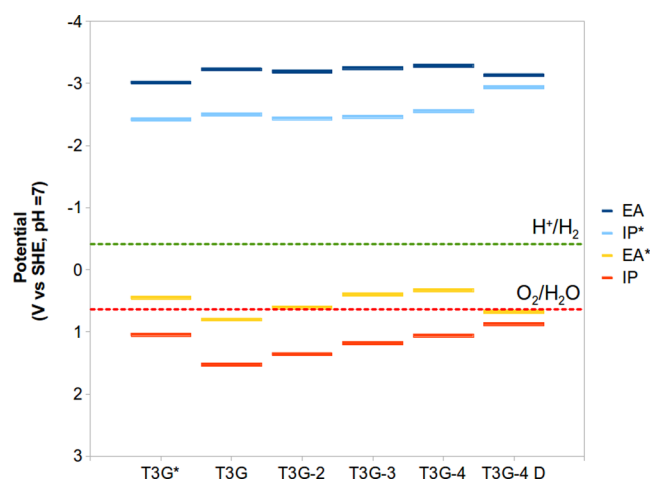
Figure 15. (TD-)B3LYP predicted IP, EA, IP*, and EA* vertical potentials of stacks of T3G in water (ε = 80.1) at pH 7. Adiabatic potentials of isolated H3G (H3G*) and T3G-4 (T3G-4 D, including Grimme D3 dispersion correction) also shown for comparison.

However, a comparison of the vertical and adiabatic potentials in Figure 15 suggests that this, in part, is an artifact resulting from the fact that the vertical potentials appear to be a worse approximation to the adiabatic potentials for these systems than in the case of the heptazine-based structures. This observation is supported by the results of (TD-)DFT-D3 calculations including the Grimme D3 dispersion correction[50] on a stack of four T3G layers. Adiabatic potentials calculated using this setup, which are now feasible as the D3 correction corrects the lack of long-range dispersive interaction between the layers in DFT, lie relatively close to the adiabatic potentials of the isolated T3G structure. The only minor catch with the (TD-)DFT-D3 calculations is that the neutral stack has a slightly larger interlayer distance than experiment, possibly because of the finite size of the stack, which also reduces the effect of stacking.

On the basis of the calculated potentials discussed above, one would expect that carbon nitride materials based on all the types of structures considered should thermodynamically be able to drive the photocatalytic reduction of protons to hydrogen. Water oxidation is also in all cases predicted to be strongly exothermic. If we trust our calculations, this suggests, as already hypothesized in our previous work where we only considered small heptazine-based cluster models,[23] that the lack of experimentally observed activity for overall water splitting by carbon nitride materials is kinetic rather than thermodynamic in origin.

The most likely origin of this kinetic issue is the fact that water oxidation to oxygen is a four-hole reaction. Oxidation of sacrificial electron donors, for example, triethylamine or methanol, is even more exothermic than water oxidation (potentials shifted by ~1 V), but crucially these are two-hole reactions. It is thus likely that electron−hole recombination prevents the buildup of a sufficient amount of holes for water oxidation and thus overall water splitting to occur, while not limiting two-hole reactions, such as methanol oxidation, to the same degree. Supporting evidence for this interpretation is the fact that in the system of carbon nitride loaded with polypyrrole nanoparticles, where overall water splitting has been demonstrated experimentally, oxidation of water to hydrogen peroxide takes place instead of to molecular oxygen, as discussed in more

detail below. The former oxidation reaction is more energetically expensive, 1.78 versus 1.23 V experimentally and 1.64 versus 1.05 V in our calculations, but is also a two-hole rather than a four-hole reaction, which might be an advantage when, as suggested above, electron−hole recombination limits the number of holes available for useful chemistry.

The Effect of Polypyrrole. Having discussed pure carbon nitride, our attention now moves to the recently reported system of carbon nitride loaded with polypyrrole nanoparticles,[18] already briefly touched upon above. While polypyrrole on its own, just like carbon nitride, displays no water splitting activity, a carbon nitride−polypyrrole mixture catalyzes the overall splitting of water into hydrogen and hydrogen peroxide.

Figure 16 shows the IP and EA potentials of both the H10G graphitic heptazine-based cluster model and a polypyrrole
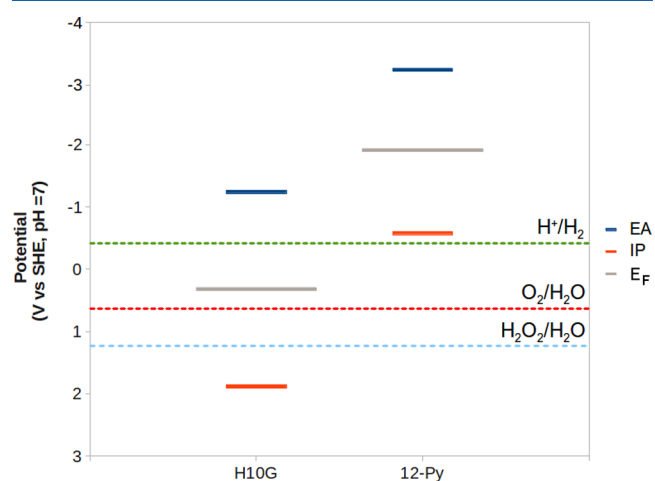
Figure 16. Comparison of the (TD-)B3LYP predicted IP and EA potentials of carbon nitride (H6G) and polypyrrole (12-Py) in water (ε = 80.1) at pH 7.

chain, 12 units long. On the basis of the potentials in Figure 16, oxidation of water to hydrogen peroxide by graphitic heptazine-based materials alone appears thermodynamically feasible at pH 7, if with a slightly low overpotential of ~0.3 V. This small driving force probably explains why, in contrast to methanol or triethylamine oxidation, which are both also two-hole reactions but with overpotentials of more than 1 V, water oxidation to hydrogen peroxide does not occur experimentally at an observable rate in the absence of polypyrrole. The EA and IP potentials of the latter in Figure 16 are dramatically shifted by more than ~2 V to more positive values, relative to the graphitic heptazine-based carbon nitrides. As a result of this shift, the reduction of protons to hydrogen by free electrons in polypyrrole is predicted to be strongly exothermic. The oxidation of water to molecular oxygen by free holes, however, appears strongly endothermic, and the oxidation of water to hydrogen peroxide even more endothermic. One would thus expect, in line with experiment, that polypyrrole on its own also does not catalyze the splitting of water, but now on strictly thermodynamic grounds. Potentials for polypyrrole chains between 4 and 16 units in the Supporting Information (Figure S14) show that these observations do not strongly depend on the exact chain size (distribution) of the polypyrrole nanoparticles.

The water oxidation activity of the carbon nitride–polypyrrole mixture thus appears to be a synergistic effect arising from the presence of both materials. A naïve interpretation of Figure 16 (and its Kohn–Sham orbital-based equivalent, Figure S15 in the Supporting Information) would suggest that this synergistic effect might arise from the fact that it is energetically advantageous for free electrons in the conduction band from polypyrrole to trickle down to the conduction band of carbon nitride and for free holes in the valence band of carbon nitride to rise up to the valence band of polypyrrole. The problem with this naïve model is that, while it allows for splitting of the exciton and spatial separation of free electrons and hole, because of the difference in chemical affinity for electrons and holes in both materials, the free holes in the valence band of polypyrrole are thermodynamically unable to oxidize water. Hence, it is difficult to see how this naïve model could explain the activity of the carbon nitride–polypyrrole mixture as water splitting catalyst.

The likely issue with the naïve model is that it ignores the semiconducting nature of both materials. As can be seen from Figure 16, the Fermi levels of the isolated intrinsic, i.e., undoped, materials ($0.5E_{VB} + 0.5E_{CB}$) are likely to be very different. When both materials are brought together in electrical contact, as they would be in the experimental photocatalyst, the Fermi levels of both materials should in principle equilibrate and a semiconductor heterojunction is formed. The Fermi level equilibration in the dark will result in a shift between the local vacuum levels on the two sides of the junction and the creation of a built-in electrical potential and electric field over the junction. The exact character and level of doping of both materials and hence the specific type of junction formed ($p–n$, $n–n$, $p–p$, $i–i$) in the experimental sample are unknown. However, we believe, based upon the alignment in Figure 16, that, after Fermi level equilibration, the built-in potential will be likely such that there will be a net negative charge on the carbon nitride side and a net positive charge on the polypyrrole side of the junction, inverting the thermodynamic preference of the free electrons and free holes in the absence of the junction. After Fermi level equilibration, the free electrons and holes are thus not only kept apart, increasing their lifetime, but also now end up on the side of the junction where they are thermodynamically able to reduce protons and oxidize water. The carbon nitride–polypyrrole photocatalyst in this scenario is an example of the wider class of heterojunction photocatalysts.[51]

CONCLUSIONS

We study the optical and photocatalytic properties of carbon nitride materials using our recently developed computational approach, based around cluster calculations. We consider structures based on heptazine and triazine and, in the latter case, both linear and graphitic topologies. Overall, we obtain a good match to experimental absorption spectra, except for graphitic triazine-based frameworks, which we hypothesize to be potentially the result of nitrogen vacancies in the experimental samples. We demonstrate that carbon nitride materials based on all three families of structures considered should under illumination be able to thermodynamically drive both reduction of protons and oxidation of water. We speculate that the lack of experimental activity of carbon nitride materials for overall water splitting is kinetic in origin and linked to electron–hole recombination limiting the number of free holes available for water oxidation. Finally, we discuss how the

experimental activity of carbon nitride–polypyrrole mixtures probably finds its origin in the formation of a junction between both materials where the built-in potential helps in keeping free electrons and holes apart.

ASSOCIATED CONTENT

Ⓢ Supporting Information

Spectra of additional conformers of cluster models of linear polymers, effect of stacking on the spectra of H3G and T3G, and potentials at pH 0 are available in the Supporting Information. This material is available free of charge via the Internet at http://pubs.acs.org.

AUTHOR INFORMATION

Corresponding Author

*E-mail: m.zwijnenburg@ucl.ac.uk. Phone: +44 (0)20 7679 4665 (M.A.Z.).

Notes

The authors declare no competing financial interest.

ACKNOWLEDGMENTS

REFERENCES

(1) Liebig, J. Uber Einige Stickstoff - Verbindungen. *Ann. Pharm.* **1834**, *10*, 1−47.

(2) Liu, A. Y.; Cohen, M. L. Prediction of New Low Compressibility Solids. *Science* **1989**, *245*, 841−842.

(3) Wang, X. C.; Maeda, K.; Thomas, A.; Takanabe, K.; Xin, G.; Carlsson, J. M.; Domen, K.; Antonietti, M. A Metal-Free Polymeric Photocatalyst for Hydrogen Production from Water under Visible Light. *Nat. Mater.* **2009**, *8*, 76−80.

(4) Jürgens, B.; Irran, E.; Senker, J.; Kroll, P.; Müller, H.; Schnick, W. Melem (2,5,8-Triamino-Tri-S-Triazine), an Important Intermediate During Condensation of Melamine Rings to Graphitic Carbon Nitride: Synthesis, Structure Determination by X-ray Powder Diffractometry, Solid-State NMR, and Theoretical Studies. *J. Am. Chem. Soc.* **2003**, *125*, 10288−10300.

(5) Lotsch, B. V.; Döblinger, M.; Sehnert, J.; Seyfarth, L.; Senker, J.; Oeckler, O.; Schnick, W. Unmasking Melon by a Complementary Approach Employing Electron Diffraction, Solid-State NMR Spectroscopy, and Theoretical Calculations—Structural Characterization of a Carbon Nitride Polymer. *Chem.—Eur. J.* **2007**, *13*, 4969−4980.

(6) Bojdys, M. J.; Muller, J. O.; Antonietti, M.; Thomas, A. Ionothermal Synthesis of Crystalline, Condensed, Graphitic Carbon Nitride. *Chem.—Eur. J.* **2008**, *14*, 8177−8182.

(7) Wang, Y.; Wang, X.; Antonietti, M. Polymeric Graphitic Carbon Nitride as a Heterogeneous Organocatalyst: From Photochemistry to Multipurpose Catalysis to Sustainable Chemistry. *Angew. Chem., Int. Ed.* **2012**, *51*, 68−98.

(8) Algara-Siller, G.; Severin, N.; Chong, S. Y.; Björkman, T.; Palgrave, R. G.; Laybourn, A.; Antonietti, M.; Khimyak, Y. Z.; Krasheninnikov, A. V.; Rabe, J. P.; et al. Triazine-Based, Graphitic

Carbon Nitride: A Two-Dimensional Semiconductor. *Angew. Chem., Int. Ed.* **2014**, *53*, 7450−7455.

(9) Wang, X.; Maeda, K.; Chen, X.; Takanabe, K.; Domen, K.; Hou, Y.; Fu, X.; Antonietti, M. Polymer Semiconductors for Artificial Photosynthesis: Hydrogen Evolution by Mesoporous Graphitic Carbon Nitride with Visible Light. *J. Am. Chem. Soc.* **2009**, *131*, 1680−1681.

(10) Yanagida, S.; Kabumoto, A.; Mizumoto, K.; Pac, C.; Yoshino, K. Poly(p-Phenylene)-Catalysed Photoreduction of Water to Hydrogen. *J. Chem. Soc., Chem. Commun.* **1985**, 474−475.

(11) Matsuoka, S.; Kohzuki, T.; Kuwana, Y.; Nakamura, A.; Yanagida, S. Visible-Light-Induced Photocatalysis of Poly(pyridine-2,5-diyl). Photoreduction of Water, Carbonyl Compounds and Alkenes with Triethylamine. *J. Chem. Soc., Perkin Trans. 2* **1992**, 679−685.

(12) Maruyama, T.; Yamamoto, T. Effective Photocatalytic System Based on Chelating Π-Conjugated Poly(2,2′-bipyridine-5,5′-diyl) and Platinum for Photoevolution of H_2 from Aqueous Media and Spectroscopic Analysis of the Catalyst. *J. Phys. Chem. B* **1997**, *101*, 3806−3810.

(13) Zhang, J.; Zhang, G.; Chen, X.; Lin, S.; Möhlmann, L.; Dołęga, G.; Lipner, G.; Antonietti, M.; Blechert, S.; Wang, X. Co-Monomer Control of Carbon Nitride Semiconductors to Optimize Hydrogen Evolution with Visible Light. *Angew. Chem., Int. Ed.* **2012**, *51*, 3183−3187.

(14) Cui, Y.; Ding, Z.; Fu, X.; Wang, X. Construction of Conjugated Carbon Nitride Nanoarchitectures in Solution at Low Temperatures for Photoredox Catalysis. *Angew. Chem., Int. Ed.* **2012**, *51*, 11814−11818.

(15) Jorge, A. B.; Martin, D. J.; Dhanoa, M. T. S.; Rahman, A. S.; Makwana, N.; Tang, J.; Sella, A.; Corà, F.; Firth, S.; Darr, J. A.; et al. H_2 and O_2 Evolution from Water Half-Splitting Reactions by Graphitic Carbon Nitride Materials. *J. Phys. Chem. C* **2013**, *117*, 7178−7185.

(16) Schwinghammer, K.; Tuffy, B.; Mesch, M. B.; Wirnhier, E.; Martineau, C.; Taulelle, F.; Schnick, W.; Senker, J.; Lotsch, B. V. Triazine-Based Carbon Nitrides for Visible-Light-Driven Hydrogen Evolution. *Angew. Chem., Int. Ed.* **2013**, *52*, 2435−2439.

(17) Ge, L.; Han, C.; Xiao, X.; Guo, L.; Li, Y. Enhanced Visible Light Photocatalytic Hydrogen Evolution of Sulfur-Doped Polymeric g-C_3N_4 Photocatalysts. *Mater. Res. Bull.* **2013**, *48*, 3919−3925.

(18) Sui, Y.; Liu, J.; Zhang, Y.; Tian, X.; Chen, W. Dispersed Conductive Polymer Nanoparticles on Graphitic Carbon Nitride for Enhanced Solar-Driven Hydrogen Evolution from Pure Water. *Nanoscale* **2013**, *5*, 9150−9155.

(19) Hong, Z.; Shen, B.; Chen, Y.; Lin, B.; Gao, B. Enhancement of Photocatalytic H_2 Evolution over Nitrogen-Deficient Graphitic Carbon Nitride. *J. Mater. Chem. A* **2013**, *1*, 11754−11761.

(20) Chu, S.; Wang, Y.; Guo, Y.; Feng, J.; Wang, C.; Luo, W.; Fan, X.; Zou, Z. Band Structure Engineering of Carbon Nitride: In Search of a Polymer Photocatalyst with High Photooxidation Property. *ACS Catal.* **2013**, *3*, 912−919.

(21) Kailasam, K.; Schmidt, J.; Bildirir, H.; Zhang, G.; Blechert, S.; Wang, X.; Thomas, A. Room Temperature Synthesis of Heptazine-Based Microporous Polymer Networks as Photocatalysts for Hydrogen Evolution. *Macromol. Rapid Commun.* **2013**, *34*, 1008−1013.

(22) Martin, D. J.; Qiu, K.; Shevlin, S. A.; Handoko, A. D.; Chen, X.; Guo, Z.; Tang, J. Highly Efficient Photocatalytic H_2 Evolution from Water Using Visible Light and Structure-Controlled Graphitic Carbon Nitride. *Angew. Chem.* **2014**, *126*, 9394−9399.

(23) Guiglion, P.; Butchosa, C.; Zwijnenburg, M. A. Polymeric Water Splitting Photocatalysts; a Computational Perspective on the Water Oxidation Conundrum. *J. Mater. Chem. A* **2014**, *2*, 11996−12004.

(24) Jorgensen, W. L.; Tirado-Rives, J. Potential Energy Functions for Atomic-Level Simulations of Water and Organic and Biomolecular Systems. *Proc. Natl. Acad. Sci. U.S.A.* **2005**, *102*, 6665−6670.

(25) Kolossváry, I.; Guida, W. C. Low Mode Search. An Efficient, Automated Computational Method for Conformational Analysis: Application to Cyclic and Acyclic Alkanes and Cyclic Peptides. *J. Am. Chem. Soc.* **1996**, *118*, 5011−5019.

(26) Vosko, S. H.; Wilk, L.; Nusair, M. Accurate Spin-Dependent Electron Liquid Correlation Energies for Local Spin Density Calculations: A Critical Analysis. *Can. J. Phys.* **1980**, *58*, 1200−1211.

(27) Lee, C.; Yang, W.; Parr, R. G. Development of the Colle-Salvetti Correlation-Energy Formula into a Functional of the Electron Density. *Phys. Rev. B* **1988**, *37*, 785−789.

(28) Becke, A. D. Density-Functional Thermochemistry. III. The Role of Exact Exchange. *J. Phys. Chem.* **1993**, *98*, 5648−5652.

(29) Stephens, P. J.; Devlin, F. J.; Chabalowski, C. F.; Frisch, M. J. Ab Initio Calculation of Vibrational Absorption and Circular Dichroism Spectra Using Density Functional Force Fields. *J. Phys. Chem.* **1994**, *98*, 11623−11627.

(30) Schäfer, A.; Horn, H.; Ahlrichs, R. Fully Optimized Contracted Gaussian Basis Sets for Atoms Li to Kr. *J. Phys. Chem.* **1992**, *97*, 2571−2577.

(31) Hirata, S.; Head-Gordon, M. Time-Dependent Density Functional Theory within the Tamm−Dancoff Approximation. *Chem. Phys. Lett.* **1999**, *314*, 291−299.

(32) Christiansen, O.; Koch, H.; Jørgensen, P. The Second-Order Approximate Coupled Cluster Singles and Doubles Model CC2. *Chem. Phys. Lett.* **1995**, *243*, 409−418.

(33) Peach, M. J. G.; Benfield, P.; Helgaker, T.; Tozer, D. J. Excitation Energies in Density Functional Theory: An Evaluation and a Diagnostic Test. *J. Chem. Phys.* **2008**, *128*, 044118.

(34) Klamt, A.; Schuurmann, G. Cosmo: A New Approach to Dielectric Screening in Solvents with Explicit Expressions for the Screening Energy and Its Gradient. *J. Chem. Soc., Perkin Trans. 2* **1993**, 799−805.

(35) Barone, V.; Cossi, M.; Tomasi, J. Geometry Optimization of Molecular Structures in Solution by the Polarizable Continuum Model. *J. Comput. Chem.* **1998**, *19*, 404−417.

(36) Schäfer, A.; Klamt, A.; Sattel, D.; Lohrenz, J. C.; Eckert, F. Cosmo Implementation in Turbomole: Extension of an Efficient Quantum Chemical Code Towards Liquid Systems. *PCCP Phys. Chem. Chem. Phys.* **2000**, *2*, 2187−2193.

(37) Trasatti, S. The Concept of Absolute Electrode Potential an Attempt at a Calculation. *J Electroanal. Chem. Interfacial Electrochem.* **1974**, *52*, 313−329.

(38) Trasatti, S. The Absolute Electrode Potential: An Explanatory Note (Recommendations 1986). *Pure Appl. Chem.* **1986**, *58*, 955−966.

(39) Zhan, C.-G.; Dixon, D. A. Absolute Hydration Free Energy of the Proton from First-Principles Electronic Structure Calculations. *J. Phys. Chem. A* **2001**, *105*, 11534−11540.

(40) Bryantsev, V. S.; Diallo, M. S.; Goddard Iii, W. A. Calculation of Solvation Free Energies of Charged Solutes Using Mixed Cluster/Continuum Models. *J. Phys. Chem. B* **2008**, *112*, 9709−9719.

(41) Ahlrichs, R.; Haser, M.; Kolmel, C.; Horn, H.; Baer, M. Electronic Structure Calculations on Workstation Computers: The program System Turbomole. *Chem. Phys. Lett.* **1989**, *162*, 165−169.

(42) Furche, F.; Ahlrichs, R. Adiabatic Time-Dependent Density Functional Methods for Excited State Properties. *J. Chem. Phys.* **2002**, *117*, 7433−7447.

(43) Furche, F.; Ahlrichs, R. Erratum: "Time-Dependent Density Functional Methods for Excited State Properties" [J. Chem. Phys. **117**, 7433 (2002)]. *J. Chem. Phys.* **2004**, *121*, 12772−12773.

(44) van Wüllen, C. Shared-Memory Parallelization of the Turbomole Programs AOFORCE, ESCF, and EGRAD: How to Quickly Parallelize Legacy Code. *J. Comput. Chem.* **2011**, *32*, 1195−1201.

(45) Schmidt, M. W.; Baldridge, K. K.; Boatz, J. A.; Elbert, S. T.; Gordon, M. S.; Jensen, J. H.; Koseki, S.; Matsunaga, N.; Nguyen, K. A.; Su, S.; et al. General Atomic and Molecular Electronic Structure System. *J. Comput. Chem.* **1993**, *14*, 1347−1363.

(46) Mohamadi, F.; Richards, N. G. J.; Guida, W. C.; Liskamp, R.; Lipton, M.; Caufield, C.; Chang, G.; Hendrickson, T.; Still, W. C. Macromodel—an Integrated Software System for Modeling Organic and Bioorganic Molecules Using Molecular Mechanics. *J. Comput. Chem.* **1990**, *11*, 440−467.

(47) Deifallah, M.; McMillan, P. F.; Corà, F. *J. Phys. Chem. C* **2008**, *112*, 5447−5453.

(48) Butchosa, C.; McDonald, T. O.; Cooper, A. I.; Adams, D. J.; Zwijnenburg, M. A. Shining a Light on *s*-Triazine-Based Polymers. *J. Phys. Chem. C* **2014**, *118*, 4314−4324.

(49) Niu, P.; Liu, G.; Cheng, H.-M. Nitrogen Vacancy-Promoted Photocatalytic Activity of Graphitic Carbon Nitride. *J. Phys. Chem. C* **2012**, *116*, 11013−11018.

(50) Grimme, S.; Antony, J.; Ehrlich, S.; Krieg, H. A Consistent and Accurate ab Initio Parametrization of Density Functional Dispersion Correction (DFT-D) for the 94 Elements H-Pu. *J. Chem. Phys.* **2010**, *132*, 154104.

(51) Jang, J. S.; Kim, H. G.; Lee, J. S. Heterojunction Semiconductors: A Strategy to Develop Efficient Photocatalytic Materials for Visible Light Water Splitting. *Catal. Today* **2012**, *185*, 270−277.

24842

dx.doi.org/10.1021/jp507372n | *J. Phys. Chem. C* 2014, 118, 24833−24842